

24

25 **Abstract**

26 A 2003 high-resolution magnetic survey conducted by the Autonomous Underwater Vehicle *ABE*
27 over the low-temperature, ultramafic-hosted hydrothermal field Lost City reveals a weak positive
28 magnetic anomaly. This observation is in direct contrast to recent observations of strong positive
29 magnetic anomalies documented over the high-temperature ultramafic-hosted hydrothermal vents
30 fields Rainbow and Ashadze, which indicates that temperature may control the production of
31 magnetization at these sites. The Lost City survey provides a unique opportunity to study a field
32 that is, to date, one of a kind, and is an end member of ultramafic-hosted hydrothermal systems.
33 Our results highlight the key contribution of temperature on magnetite production resulting from
34 serpentinization reactions. Whereas high temperature promotes significant production and
35 partitioning of iron into magnetite, low temperature favors iron partitioning into various alteration
36 phases, resulting in a magnetite-poor rock. Moreover, the distribution of magnetic anomalies
37 confirms results of a previous geological survey indicating the progressive migration of
38 hydrothermal activity upslope. These discoveries contribute to the results of 25 years of magnetic
39 exploration of a wide range of hydrothermal sites, from low- to high-temperature and from
40 basalt- to ultramafic-hosted, and thereby validate using high-resolution magnetics as a crucial
41 parameter for locating and characterizing hydrothermal sites hosting unique chemosynthetic-
42 based ecosystems and potentially mineral-rich deposits.

43

44 **1) Introduction**

45 The discovery of hydrothermal activity along the Galapagos Rift (Corliss et al., 1979) paved the
46 way for large-scale, deep-sea exploration of oceanic ridges, revealing a myriad of hydrothermal
47 vent fields primarily hosted on basaltic crust, with lesser gabbroic and ultramafic material (Kelley

48 and Shank, 2010). In contrast to intermediate- and fast-spreading systems where basaltic rocks
49 dominate, along slow- to ultraslow-spreading centers, the tectonically-dominated geology
50 (Karson and Elthon, 1987; Tucholke et al., 1998; Escartin et al., 2008) gives rise to a higher
51 abundance of hydrothermal systems hosted by variable amounts of ultramafic and gabbroic
52 material, such as the well-known Rainbow and Ashadze hydrothermal fields (Charlou et al.,
53 2002; Charlou et al., 2010; Fouquet et al., 2008). These high-temperature venting systems
54 (>350°C) are characterized by sulfide chimneys emitting low pH fluids rich in carbon dioxide,
55 methane and hydrogen; chemical signatures that are hallmarks of fluid interaction with mafic and
56 ultramafic material in the subsurface (Charlou et al., 2002; Fouquet et al., 2010; Kelley and
57 Shank, 2010; Ohara et al., 2012).

58 Although the magnetic signature of basalt-hosted hydrothermal sites is well constrained (Tivey et
59 al., 1993; Tivey and Johnson, 2002; Tivey and Dymont, 2010; Szitkar et al., 2014a; Szitkar et al.,
60 2015), that of ultramafic-hosted hydrothermal sites (UMHS) remains comparatively poorly
61 studied and hence understood. Indeed, only the study by Szitkar et al. (2014b) of the Rainbow
62 and Ashadze UMHS reveals that these high-temperature systems composed of variable mixtures
63 of ultramafic, gabbroic and basaltic material are associated with a strong magnetization, implying
64 that a specific set of seafloor thermal-chemical processes are in play. Within these previously
65 studied, high-temperature systems, mineral-fluid reactions and the formation and alteration of
66 magnetic minerals are influenced by both temperature and the diverse rock compositions (Toft et
67 al., 1990). To better understand magnetization processes in an ultramafic-dominated system
68 characterized by low- to moderate- fluid temperatures, a detailed magnetic survey of the off-axis
69 Lost City Hydrothermal Field (LCHF) was undertaken in 2003 by the Autonomous Underwater
70 Vehicle *ABE* (MAR, 30°N). This unique field, which issues high-pH fluids at temperatures up to
71 116°C (Seyfried et al., 2015), is in stark contrast to the high-temperature Rainbow-like UMHS,

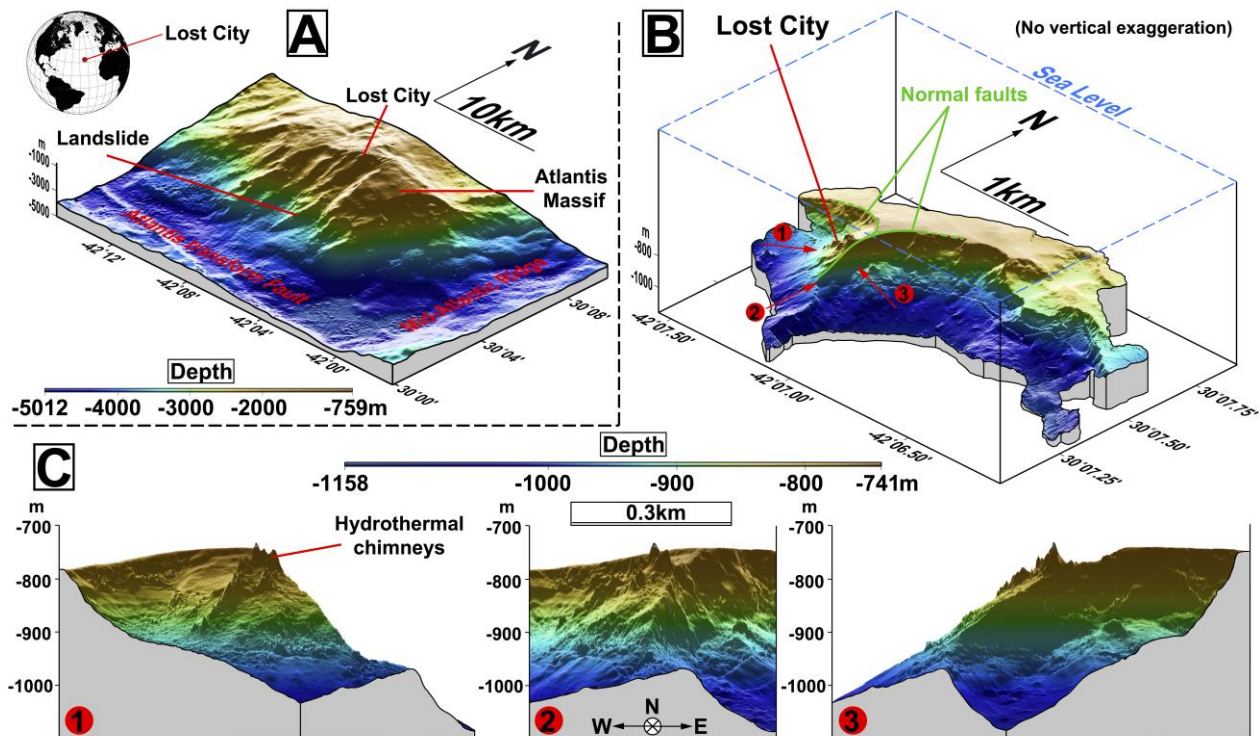
72 thus it provides an ideal end-member hydrothermal system to constrain the source of
73 magnetization in ultramafic environments.

74

75 2) Geological context

76 The LCHF is located near the summit of the southern wall of the Atlantis Massif, an oceanic core
77 complex marking the inside corner of the intersection between the Mid-Atlantic Ridge and the
78 Atlantis Transform Fault (30°N) (Kelley et al., 2001; Kelley et al., 2005; Kelley and Shank,
79 2010; Blackman et al., 2002; Karson et al., 2006; Denny et al., 2015). The site sits at ~750 m
80 depth, 15 km away from the spreading axis (Fig. 1A), on a south-facing spur west of a sub-
81 vertical fault (Figs. 1A and B) (Kelley et al., 2001).

82



83

84 **Fig. 1:** Bathymetry of the LCHF. (A) Regional, ship-based bathymetry of the Atlantis Massif, at the inside corner of
85 the intersection between the Mid-Atlantic Ridge and the Atlantis Transform Fault. (B) Detailed bathymetry of Lost

86 City and its surroundings. (C) Lost City seen from various angles, respectively corresponding to the red arrows on B.
87 The Poseidon complex and the near vertical cliff marking the fault immediately east of the site are clearly apparent.
88
89 The LCHF is unique to date because it is one of only two low- to moderate- temperature UMHS
90 known (Ohara et al., 2012). It is the only field with massive carbonate hydrothermal structures
91 actively venting high-pH fluids (Fouquet et al., 2010) at temperatures up to 116°C (Seyfried et
92 al., 2015). Fluid temperatures at depth range from 110°C to 250°C (Kelley et al., 2001; Kelley et
93 al., 2005; Früh-Green et al., 2003; Proskurowski et al., 2006; Foustoukos et al., 2008). Moreover,
94 hydrothermal activity is likely a consequence of both exothermic chemical reactions occurring
95 beneath the field between seawater and peridotite rocks, and lithospheric cooling (Kelley et al.,
96 2005). The low- to moderate temperature serpentinization produces the observed high-pH fluids
97 enriched in low molecular weight hydrocarbons and high hydrogen concentrations (Kelley et al.,
98 2005; Proskurowski et al., 2006; Proskurowski et al., 2008).

99 The core of the field is dominated by the 60 m tall Poseidon complex that forms linear, ~300 m
100 long, east-west trending structure consisting of carbonate minerals and variable amounts of
101 brucite (Fig. 1C) (Kelley et al., 2005). Two extinct fields occur ~300 m downslope and ~450 m
102 west of Poseidon proper (Denny et al., 2015). The intensity of hydrothermal activity rapidly
103 decreases away from the core of the field. Hydrothermal venting on the east side of the field
104 occurs along cockscomb-like structures on the edge of a high-angle normal fault, and as diffuse
105 flow issuing from highly faulted rocks on a near-vertical cliff marking the fault. The
106 southernmost summit of the massif is marked by carbonate-filled fissures cutting the pelagic
107 caprock that are thought to be sites of nascent venting (Kelley et al., 2005; Denny et al., 2015).

108 Compared to other known hydrothermal sites, the LCHF is surrounded by extremely steep terrain
109 resulting from a complex fault network and associated mass wasting (Karson et al., 2006; Denny

110 et al., 2015).

111

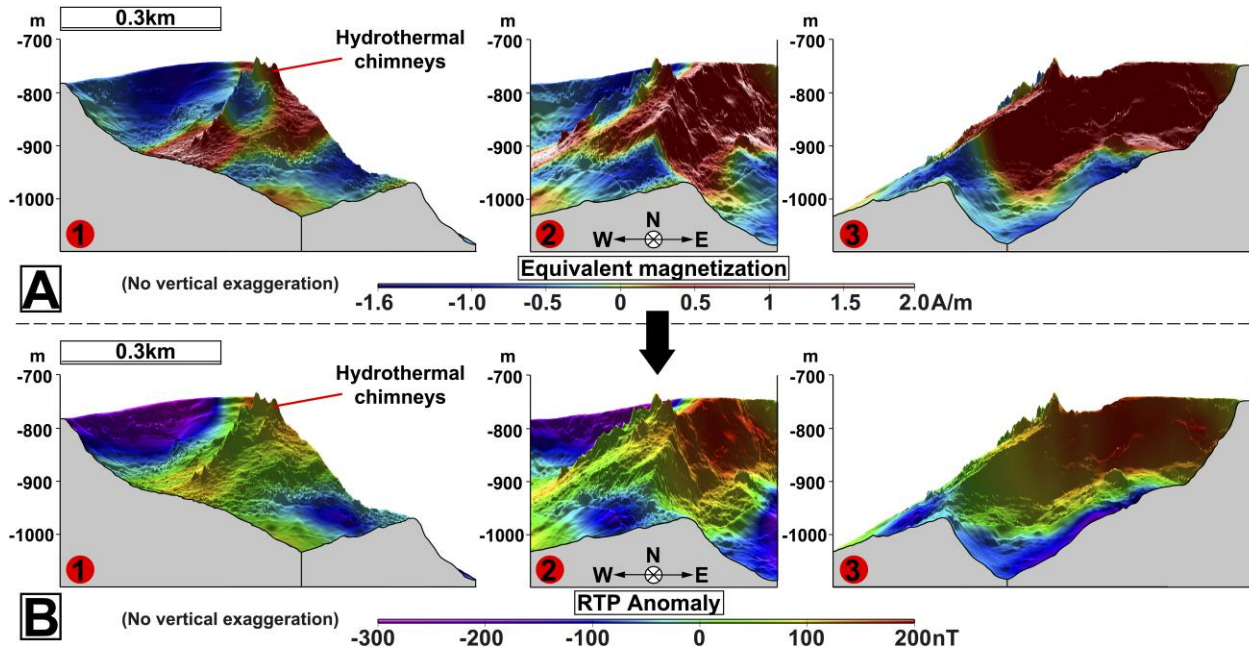
112 **3) Methods and Results**

113 High-resolution magnetic and bathymetric data were collected by the Autonomous Underwater
114 Vehicle (AUV) *ABE* during cruise AT7-34 of R/V *Atlantis* in 2003. The three components of the
115 magnetic field were acquired at 1 Hz sample rate using a fluxgate magnetometer mounted on the
116 AUV frame. To survey the site and its surroundings, *ABE* carried out seventeen dives with
117 tracklines roughly following the isobaths.

118 The AUV magnetic influence is removed from the data using a calibration method proposed by
119 Isezaki (1986) and Honsho et al. (2009) to resolve the crustal magnetic anomaly. Additionally,
120 because of the geomagnetic field inclination and declination, magnetic anomalies are phase-
121 shifted, i.e., not centered above their causative sources. To eliminate this phase-shift, we use
122 Reduction to the Pole (RTP). This transformation is problematic, however, in this strongly 3D
123 environment. Indeed, the direct RTP is achieved in the Fourier domain and requires the data to be
124 collected on a level datum plane, which is not feasible for this dataset. Consequently, the
125 anomalies either have to be upward-continued to a plane located above the shallowest point of the
126 survey (Guspi, 1987), which would act as a low-pass filter and overly smooth the magnetic
127 response, or we must invert the anomalies into an equivalent magnetization and estimate the RTP
128 in the geometry of the experiment using a vertical geomagnetic field. Because traditional
129 inversion methods are also performed in the spectral domain (Parker and Huestis, 1974), the
130 over-filtering problem remains and details are lost. The new Bayesian inversion method
131 developed by Honsho et al., (2012) and specifically designed for near-seafloor datasets acquired
132 along uneven routes represents the most effective method to obtain a rigorous RTP anomaly
133 while preserving the short wavelengths. The magnetization is estimated along the tracks of the

134 submersible, preserving the high-resolution signals. The result of this inversion is displayed in
135 Fig. 2A and the corresponding RTP anomaly in Fig. 2B.

136



137

138 **Fig. 2:** Equivalent magnetization and magnetic anomaly of the LCHF (Same projections as in Fig. 1C). (A)
139 Equivalent magnetization resulting from the Bayesian inversion and draped on the site high-resolution bathymetry.
140 (B) RTP anomaly recomputed in the geometry of the experiment using this magnetization and a vertical geomagnetic
141 field. The Poseidon complex and the northeastern fault are associated with the highest anomaly amplitude, whereas
142 the rest of the site is characterized by weak positive magnetic signature.

143

144 The magnetic inversion reveals a relatively weak magnetization contrast and the recomputed
145 Reduced-to-the-Pole (RTP) magnetic anomaly is characterized by low amplitude. The study by
146 Szitkar et al. (2014b) reveals that high-temperature systems with variable amounts of ultramafic
147 to basaltic material are associated with variably strong positive magnetization, depending on the
148 site dimensions and the amount of magnetized material. The LCHF is comparable in size to the
149 high-temperature UMHS Rainbow (2014b), however its bedrock equivalent magnetization is

150 considerably weaker, yet marginally stronger than the surrounding rocks. These results, therefore,
151 suggest a different intrinsic magnetization of basement rocks proximal to the plumbing system
152 beneath the field proper. The strongest positive anomaly extends over the Poseidon area and
153 upslope along the major north-south oriented fault that bounds the field to the east. Farther west,
154 the anomaly rapidly decreases, but still remains stronger than in the vicinity of the site. At the
155 bottom of the western slope, the anomaly again increases slightly (Fig. 2B).

156

157

158 **4) Discussion**

159 The positive magnetization contrast at high-temperature UMHS is interpreted to be a
160 combination of: 1) strongly magnetized magnetite produced by high-temperature seafloor
161 serpentinization reactions (Szitkar et al., 2014b); 2) the volume and concentration of magnetized
162 material; and 3) the reducing properties of hydrothermal fluids preserving magnetite within the
163 plumbing system from oxidation (Fouquet et al., 2010). In contrast, the magnetite located in the
164 surrounding terrain is subject to low-temperature seawater oxidation and converted into less
165 magnetic minerals (Szitkar et al., 2014b).

166 By studying the RTP anomaly over the LCHF, the shape of the underlying plumbing system with
167 reference to its magnetite distribution and physical characteristics can be constrained. The
168 intensity of magnetite magnetization is subject to the strength of the magnetizing field (i.e.
169 paleointensity), grain size, and domain state (Dunlop and Prévot, 1982; Cullity and Graham,
170 2009). Evidence for magnetic grain-size dependence with the degree of serpentinization is
171 lacking (Oufi et al., 2002; Malvoisin et al., 2012), therefore we assume that magnetite formed
172 beneath the LCHF and Rainbow share comparable fine-scale physical properties. The amplitude
173 of the magnetic anomaly is therefore believed to mainly depend on the magnetite concentration

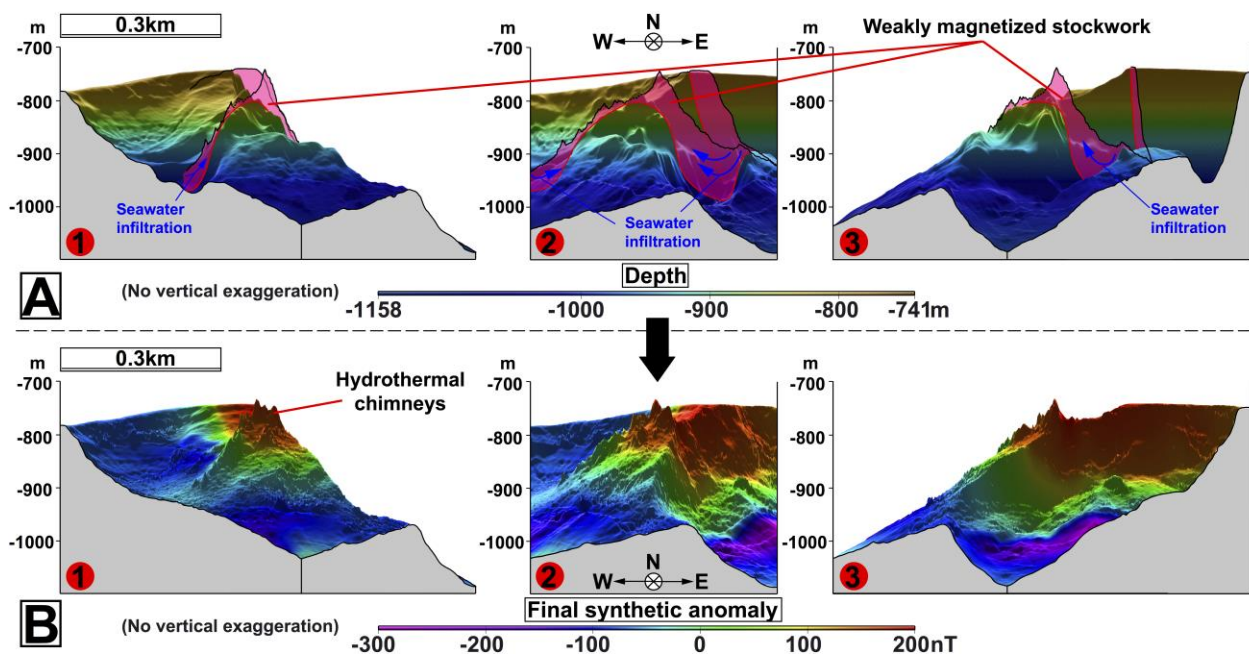
174 within the rocks, which, in turn, can be influenced by temperature, oxidation processes,
175 water/rock ratios, and/or Fe partitioning into brucite or other alteration phases (Früh-Green et al.,
176 1996; Früh-Green et al., 2004; Andreani et al., 2013; Klein et al., 2014).

177 In this study, a nested forward modeling approach was used to examine various hypotheses on
178 factors controlling the strength of the magnetic anomaly, until results were achieved that
179 reproduced the data (Fig. 2B). To investigate the role of topography in generating magnetic
180 anomalies we compute the magnetic field response of a uniformly, 1A/m magnetized seafloor
181 using the geometry of the experiment. The result of this modeling confirms that the seafloor
182 topography alone is not sufficient to account for the observed anomalies (Fig. S1), and additional
183 sources of magnetization are therefore required.

184 Magnetic forward models are impacted by a combination of at least three parameters: the seafloor
185 magnetization, the thickness of the magnetized layer and the existence of a non-magnetic deposit
186 covering or within the magnetized basement. To estimate the seafloor magnetization and to
187 constrain the shape of magnetite distribution, we use geometrical considerations. The ridge on
188 which the LCHF is located corresponds to the intersection of two normal faults (Denny et al.,
189 2015), focusing fluid ascent (Kelley et al., 2005; Karson et al., 2006; Ludwig et al., 2006) (Fig.
190 1B). We assume a uniformly magnetized seafloor and iterate towards a synthetic anomaly
191 comparable to the observed one by adjusting the shape of the magnetite distribution. The result is
192 non-realistic, as an infinitely thick, 1 A/m plumbing system does not generate the correct
193 anomaly amplitude (Fig. S2).

194 The high-angle normal fault east of the Poseidon area is approximately 200 m high. Moreover,
195 the depth of the sources visible on magnetic anomalies directly correlates with the altitude of the
196 measurements. As our data were collected roughly 70 m above the seafloor, dominating
197 anomalies are generated at maximal depths of 200 to 300 m. We therefore suggest that the upflow

198 zone producing the positive anomaly has a similar height, with seawater seeping where the high-
 199 angle fault intersects the seafloor (Fig. 3A and 4A). To the west, the fault plane is less steep and
 200 observations suggest that hydrothermal discharge is weak, which could infer that a lesser amount
 201 of magnetite has formed in this area. Considering these hypotheses, we contour the fabric
 202 geometry (Fig. 3A) to produce an anomaly with a satisfying shape but still far from the correct
 203 amplitude.
 204



205 **Fig. 3:** Geometry of the magnetite distribution at LCHF (Same projections as in Fig. 1C). (A) Contour of the
 206 plumbing system lower interface with reference to its magnetite distribution along two across-site profiles (red lines),
 207 producing an anomaly with a satisfying shape. The high-resolution bathymetry outline (black lines) is also added.
 208 Seawater infiltration occurs at the faults intersection with the seafloor and a weakly magnetized plumbing system is
 209 sufficient to account for the observed anomaly amplitude. (B) Synthetic anomaly produced in the geometry of the
 210 experiment assuming a vertical geomagnetic field and a 2 A/m magnetized plumbing system. This model fits with
 211 the observed RTP anomaly and reveals low magnetite concentration resulting from low-temperature serpentinization
 212 reactions.
 213
 214

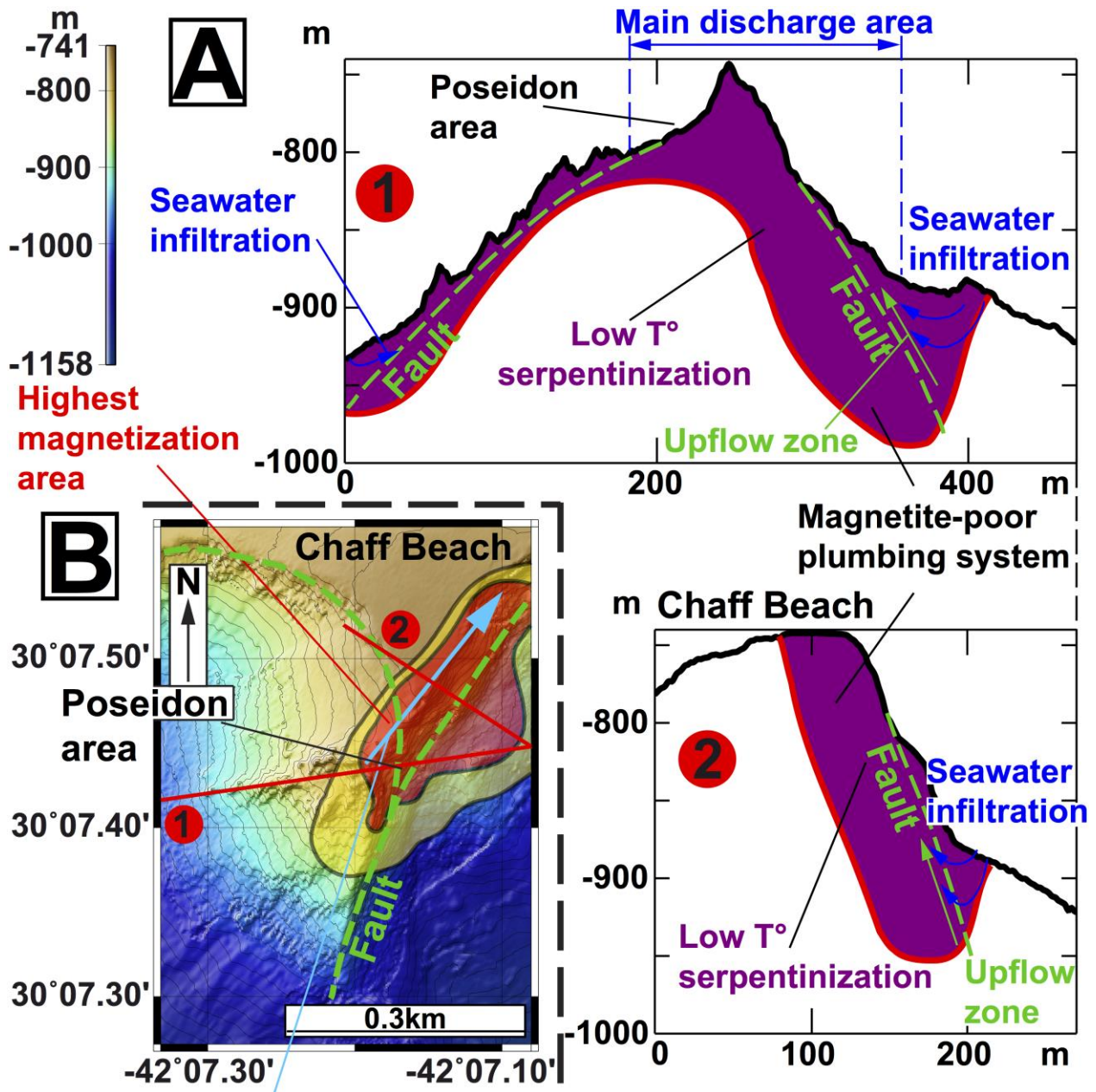
215 The last possible option consists of investigating the magnetite concentration within the rock, and
216 recovered basement samples already reveal that magnetite is common, but not pervasive.
217 Although its concentration cannot be unambiguously directly inferred through modeling, a
218 comparison with high-temperature UMHS can be achieved by a variable magnetization with the
219 final models being displayed in Fig. 3B and 4A along two across-site profiles. To account for
220 both the shape and amplitude of the observed RTP anomaly, a magnetite-rich domain of
221 serpentinization must be located under the Poseidon area and extend uphill, along the eastern
222 fault. Moreover, the model reveals that serpentinite produced by the low-temperature
223 serpentinization reaction would have to be weakly magnetized; 2 A/m is enough to generate the
224 observed anomaly amplitude. Nevertheless, as the magnetite magnetization does not depend on
225 the serpentinization degree, the origin of the weak magnetic signature can only result from its
226 concentration within the host rock. Studies of Allen and Seyfried (2003), Klein et al. (2009,
227 2014), McCollom and Bach (2009), and Malvoisin et al. (2012) reveal that low-temperature
228 serpentinization favors brucite formation rather than magnetite below 150°C, resulting in a
229 magnetite-poor (i.e., less magnetic) rock, while high-temperature serpentinization is associated
230 with magnetite formation and thus a more magnetic rock. However, no brucite has been found
231 within the serpentinized basement rocks of the Atlantis Massif. Instead, the serpentinites are
232 commonly oxidized and contain gabbroic lenses and impregnations. In addition, Si-
233 metasomatism is prevalent, occurring as talc-amphibole-chlorite zones within the serpentinites
234 (Boschi et al., 2006).

235 In comparison with the Rainbow samples that have a maximum magnetization of ~30 – 35 A/m
236 (Szitkar et al., 2014b), magnetite within Lost City plumbing system appears to be at least fifteen
237 times less intense based on the inversion results. The difference in magnetic characteristics
238 between Rainbow and Lost City may therefore largely reflect the role of temperature and fluid

239 composition in the production/consumption of magnetite during serpentinization reactions,
240 metasomatism and oxidation, and explains the origin of the weak magnetic anomaly amplitude
241 associated with the LCHF.

242 The highest magnetization contrast at the LCHF is located under the Poseidon area, but also
243 encompasses the fault to the northeast and the easternmost part of Chaff Beach (Denny et al,
244 2015), marking the top of the spur (Fig. 4B). Such observations reveal that the current active zone
245 of serpentinization and magnetite formation extends upslope, beyond the limits of the main
246 hydrothermal complex, consistent with the diffuse venting observed in this area (Kelley et al.,
247 2001; Denny et al, 2015). To the west, there is a weakly positive magnetic anomaly, in
248 accordance with weak hydrothermal activity, i.e., the magnetite located in this part of the
249 plumbing system is likely to be less abundant than that of the Poseidon and fault areas. The
250 progressive decrease in reduced, focused fluids could allow for more diffuse and oxidized fluids
251 to circulate in the basement and thus promote the alteration of magnetite or the precipitation of
252 less or non-magnetic minerals. However, magnetite produced under the current main active site
253 still benefits from the reducing conditions associated with active serpentinization, and therefore
254 retains a stronger magnetization. Along the fault, the high magnetization suggests that a higher
255 temperature phase has created a magnetite body, which, combined with the nascent venting,
256 supports the hypothesis of a progressive shift of hydrothermal activity uphill proposed by Denny
257 et al. (2015).

258



Propagation of hydrothermal activity

259
 260 **Fig. 4:** Sections of the LCHF showing the potential propagation of hydrothermal activity. (A) Proposed geometry of
 261 the plumbing system along the two across-site profiles. Seawater infiltration initiates low-temperature
 262 serpentinization reaction, i.e., the production of a small amount of magnetite. (B) map view of the site. The highest
 263 magnetization area encompasses the Poseidon complex and the fault to the northeast, suggesting a progressive shift
 264 of hydrothermal activity upslope.
 265

266 **5) Conclusions**

267 High-resolution, near-seafloor magnetic data reveal that the LCHF is associated with a weak
268 positive anomaly. This observation is consistent with the typical magnetic signature of other
269 UMHS discovered to date, and therefore confirms that UMHS exhibit a magnetic signature
270 opposite to that of basalt-hosted sites. However, the relative weakness of the magnetic response
271 of bedrock at the LCHF likely reflects a lower concentration of magnetite produced during low-
272 temperature serpentinization reactions and the fact that Si-metasomatism is prevalent in the
273 basement rocks underlying the field. Temperature and fluid chemistry are therefore crucial
274 parameters controlling the characteristics of the plumbing systems at UMHS: high-temperature
275 favors the creation of high magnetite concentrations. At low temperature and/or in the presence
276 of hydrothermal fluids, iron can be partitioned into non-magnetic brucite, serpentine, chlorite,
277 talc and amphibole and lead to the production of considerably lower concentrations of magnetite,
278 and thus, a weakly magnetized plumbing system. Moreover, magnetic anomalies are consistent
279 with the suggestion that hydrothermal activity at Lost City is progressively moving upslope,
280 confirming that the location of discharge sites evolve during the lifetime of hydrothermal
281 systems. Our study finally underlines the usefulness of magnetic surveys in identifying and
282 characterizing ultramafic-hosted hydrothermal systems that host distinctive chemosynthetic-
283 based ecosystems (Shock and Schulte, 1998) and potentially rich mineral deposits (Fouquet et al.,
284 2010).

285

286

287

288

289

290 **Acknowledgements**

291 We thank the captain and crew of R/V *Atlantis* and the technical team of the AUV *ABE* for
292 excellent work at sea. We especially thank Dana Yoerger for having processed the high-
293 resolution bathymetric data used in this study. Chie Honsho deserves our gratitude for offering us
294 the opportunity to use her ABIC inversion method to perform the reduction to the pole. Geomar,
295 Helmholtz Centre for Ocean Research (Kiel, Germany) supported this research.

296

297

298 **References**

299

300 Allen, D. E., Seyfried, W. E., 2003. Compositional controls on vent fluids from ultramafic-hosted
301 hydrothermal systems at mid-ocean ridges: An experimental study at 400°C, 500 bars.
302 *Geochimica Cosmochimica Acta* 67: 1531–1542.

303

304 Andreani, M., Munoz, M., Marcaillou, C., Delacour, A., 2013. μ XANES study of iron redox state
305 in serpentine during oceanic serpentinization. *Lithos* 178: 70–83, doi: 10.1016/j.lithos.2013
306 .04.008.

307

308 Blackman, D. K. and 12 others, 2002. Geology of the Atlantis Massif (Mid-Atlantic Ridge,
309 30°N): Implications for the evolution of an ultramafic oceanic core complex. *Marine*
310 *Geophysical Researches* 23: 443–469, doi: 10.1023/B:MARI.000 0018232.14 085.75.

311

312 Boschi, C., Früh-Green, G. L., Delacour, A., Karson, J. A., Kelley, D. S., 2006. Mass transfer and
313 fluid flow during detachment faulting and development of an oceanic core complex, Atlantis
314 Massif (MAR 30°N). *Geochem. Geophys. Geosyst.* 7 : Q01004, doi:10.1029/2005GC001074.
315

316 Charlou, J. L., Donval, J. P., Fouquet, Y., Jean-Baptiste, P., Holm, N., 2002. Geochemistry of
317 high H₂ and CH₄ vent fluids issuing from ultramafic rocks at the Rainbow hydrothermal field
318 (36.14°N, MAR). *Chemical Geology* 191(4): 345–359.
319

320 Charlou, J. L., Donval, J. P., Konn, C., Ondreas, H., Fouquet, Y., 2010. High production of H₂
321 and CH₄ and evidence of abiotic hydrocarbons synthesis by serpentinization in ultramafic-hosted
322 hydrothermal systems on the Mid-Atlantic Ridge. *American Geophysical Union Geophysical*
323 *Monograph Series* 188: 265–296.
324

325 Corliss, J. B., and 10 others, 1979. Submarine thermal springs on the Galapagos Rift. *Science*
326 203: 1073–1083, doi: 10.1126/science.203.4385.1073.
327

328 Cullity, B. D., Graham, C. D., 2009. Introduction to Magnetic Materials, New York: Wiley–
329 IEEE. p. 116, ISBN 0-471-47741-9.
330

331 Denny, A. R., Kelley, D. S., Früh-Green, G. L., 2015. Geologic Evolution of the Lost City
332 Hydrothermal Field. *Geochem. Geophys. Geosyst.* 17: 375–394, doi: 10.1002/2015GC005869.
333

334 Dunlop, D. J., Prévot, M., 1982. Magnetic properties and opaque mineralogy of drilled submarine
335 intrusive rocks. *Geophysical Journal of the Royal Astronomical Society* 69: 763–802.

336

337 Escartin, J., Smith, D. K., Cann, J., Schouten, H., Langmuir, C. H., Escrig, S., 2008. Central role
338 of detachment faults in accretion of slow-spreading oceanic lithosphere. *Nature* 455: 790–794,
339 doi: 10.1038/nature07333.

340

341 Fouquet, Y., and 26 others, 2008. Serpentine cruise ultramafic-hosted hydrothermal deposits on
342 the Mid-Atlantic Ridge; first submersible studies on Ashadze 1 and 2, Logatchev 2 and Krasnov
343 vent fields. *InterRidge News* 17: 15–19.

344

345 Fouquet, Y., and 13 others, 2010. Geodiversity of hydrothermal processes along the Mid-Atlantic
346 Ridge ultramafic-hosted mineralization: A new type of oceanic Cu-Zn-Co-Au VMS deposit.
347 *American Geophysical Union Geophysical Monograph Series* 188: 321–368.

348

349 Foustoukos, D. I., Savov, I. P., Janecky, D. R., 2008. Chemical and isotopic constraints on
350 water-rock interactions at the Lost City hydrothermal field, 30°N, Mid-Atlantic Ridge.
351 *Geochimica et Cosmochimica Acta* 72(22), 5457–5474.

352

353 Früh-Green, G. L., Plas, A., Lecuyer, C., 1996. Petrologic and stable isotopic constraints on
354 hydrothermal alteration and serpentinization of the EPR shallow mantle at Hess Deep, Site 895,
355 in Mevel, C., et al. *Proceedings of the Ocean Drilling Program, Scientific results* 147: College
356 Station, Texas, Ocean Drilling Program, 109–163, doi: 10.2973/odp.proc.sr.147.016.1996.

357

358 Früh-Green, G. L., and 7 others, 2003. 30 000 Years of Hydrothermal Activity at the Lost City
359 Vent Field. *Science* 301(5632): 495–498.

360

361 Früh-Green, G. L., Connolly, J. A. D., Plas, A., Kelley, D. S., Grobéty, B., 2004. Serpentinization
362 of oceanic peridotites: implications for geochemical cycles and biological activity. In *The*
363 *Subseafloor Biosphere at Mid-ocean Ridges* 144 (eds. W. S. D. Wilcock, E. F. DeLong, D. S.
364 Kelley, J. A. Baross and S. C. Cary): American Geophysical Union, Washington, D.C., 119–136.

365

366 Guspi, F., 1987. Frequency-domain reduction of potential field measurements to a horizontal
367 plane. *Geoexploration* 24: 87–98, doi: 10.1016/0016-7142(87)90083-4.

368

369 Honsho, C., Dymant, J., Tamaki, K., Ravilly, M., Horen, H., Gente, P., 2009. Magnetic structure
370 of a slow spreading ridge segment : Insights from a near-bottom magnetic measurements onboard
371 a submersible. *J. Geophys. Res.* 114: B05101, doi: 10.1029/2008 JB005915.

372

373 Honsho, C., Uta, T., Tamaki, K., 2012. The inversion of deep-sea magnetic anomalies using
374 Akaike)s Bayesian information criterion. *J. Geophys. Res.* 117, doi: 10.1029/2011JB008611.

375

376 Isezaki, N., 1986. A new shipboard three-component magnetometer. *Geophysics* 51: 1992–1998,
377 doi: 10/1190/1.1442054.

378

379 Karson, J. A., Elthon, D., 1987. Evidence for variations in magma production along oceanic
380 spreading centers; a critical appraisal. *Geology* 7(2): 127–131.

381

382 Karson, J. A., Früh-Green, G. L., Kelley, D. S., Williams, E. A., Yoerger, D. R., Jakuba, M.,
383 2006. Detachment shear zone of the Atlantis Massif core complex, Mid-Atlantic Ridge, 30°N:
384 *Geochem. Geophys. Geosyst.* 7, doi: 10.1029/2005GC001109.
385

386 Kelley, D. S., and 11 others, 2001. An off-axis hydrothermal vent field near the Mid-Atlantic
387 Ridge at 30°N. *Nature* 412: 145–149, doi: 10.1038/35084000.
388

389 Kelley, D. S., and 25 others, 2005. A serpentinite-hosted ecosystem: the Lost City hydrothermal
390 field. *Science* (New York, N.Y.) 307: 1428–1434, doi: 10.1126 /science.1102556.
391

392 Kelley, D. S., Shank, T. M., 2010. Hydrothermal systems: A decade of discovery in slow
393 spreading environments. *Geophysical Monograph Series* 188: 369–407, doi: 10. 1029
394 /2010GM000945.
395

396 Klein, F., Bach, W., Jöns, N., McCollom, T., Moskowitz, B., Berquo, T., 2009. Iron partitioning
397 and hydrogen generation during serpentinization of abyssal peridotites from 15°N on the Mid-
398 Atlantic Ridge. *Geochimica et Cosmochimica Acta* 73: 6868–6893.
399

400 Klein, F., Bach, W., Humphris, S. E., Kahl, W. A., Jons, N., Moskowitz, B., Berquo, T., 2014.
401 Magnetite in seafloor serpentinite – Some like it hot. *Geology* 42: 135–138.
402

403 Ludwig, K. A., Kelley, D. S., Butterfield, D. A., Nelson, B. K., Früh-Green, G. L., 2006.
404 Formation and evolution of carbonate chimneys at the Lost City Hydrothermal Field. *Geochimica*
405 *et Cosmochimica Acta* 70: 3625–3645, doi: 10.1016/j.gca2006.04. 016.

406

407 Malvoisin, B., Brunet, F., Carlut, J., Rouméjon, S., Cannat, M., 2012. Serpentinization of oceanic
408 peridotites: 2. Kinetics and processes of San Carlos olivine hydrothermal alteration. *J. Geophys.*
409 *Res.* 117: B04102, doi: 10.1029/2011JB008842.

410

411 McCollom, T. M., Bach, W., 2009. Thermodynamic constraints on hydrogen generation during
412 serpentinization of ultramafic rocks. *Geochimica Cosmochimica Acta* 73: 856–875.

413

414 Ohara, Y., and 13 others, 2012. A serpentinite-hosted ecosystem in the Southern Mariana
415 Forearc. *Proc Natl Acad Sci USA* 109(8): 2831–2835.

416

417 Oufi, O., Cannat, M., Horen, H., 2002. Magnetic properties of variably serpentinized abyssal
418 peridotite. *J. Geophys. Res.*, 107: 3–19, doi:10.1029/2001JB000549.

419

420 Parker, R. L., Huestis, S. P., 1974. The inversion of magnetic anomalies in the presence of
421 topography. *J. Geophys. Res.* 79: 1587–1593.

422

423 Proskurowski, G., Lilley, M. D., Kelley, D. S., Olson, E. J., 2006. Low temperature volatile
424 production at the Lost City hydrothermal field, evidence from a hydrogen stable isotope
425 geothermometer. *Chemical Geology* 229(4): 331–343.

426

427 Proskurowski, G. and 7 others, 2008. Abiogenic hydrocarbon production at Lost City
428 hydrothermal field. *Science* 319(5863): 604–607.

429

430 Seyfried, W. E., Pester, N. J., Tutolo, B. M., Ding, K., 2015. The Lost City hydrothermal system:
431 Constraints imposed by vent fluid chemistry and reaction path models on subseafloor heat and
432 mass transfer processes. *Geochimica et Cosmochimica Acta* 163(15): 59–79.

433
434 Shock, E. L., Schulte, M. D., 1998. Organic synthesis during fluid mixing in hydrothermal
435 systems. *J. Geophys. Res.* 103(12): 513–527.

436
437 Szitkar, F., Dymant, J., Fouquet, Y., Choi, Y., 2014a. What causes low magnetization at basalt-
438 hosted hydrothermal sites? Insights from inactive site Krasnov (MAR 16°38'N): *Geochem.*
439 *Geophys, Geosyst.* 15: 1441–1451, doi: 10.1002/2014GV00528 4.

440
441 Szitkar, F., Dymant, J., Fouquet, Y., Honsho, C., Horen, H., 2014b. The magnetic signature of
442 ultramafic-hosted hydrothermal sites. *Geology* 42: 715–718.

443
444 Szitkar, F., Petersen, S., Caratori Tontini, F., Cocchi, L., 2015. High-resolution magnetics reveal
445 the deep structure of a volcanic arc-related basalt-hosted hydrothermal site (Palinuro, Tyrrhenian
446 Sea). *Geochem. Geophys, Geosyst.* 16, doi: 10.1002/ 2015GC005769.

447
448 Tivey, M. A., Rona, P. A., Schouten, H., 1993. Reduced crustal magnetization beneath the active
449 sulfide mound, TAG hydrothermal field, Mid-Atlantic Ridge, 26°N. *Earth and Planetary Science*
450 *Letters* 115: 101–115, doi: 10.1016 /0012-821X(93)90216-V.

451

452 Tivey, M. A., Johnson, H. P., 2002. Crustal magnetization reveals subsurface structure of Juan de
453 Fuca Ridge hydrothermal vent fields. *Geology* 30: 979–982, doi: 10.1130/ 0091-
454 7613(2002)030<0979 :CMRSSO>2.0.CO ;2.

455
456 Tivey, M. A., Dymant, J., 2010. The magnetic signature of hydrothermal systems in slow-
457 spreading environments. *American Geophysical Union, Geophysical Monograph Series* 188: 43–
458 66.

459
460 Toft, P. B., Arkani-Hamed, J., Haggerty, S. E., 1990. The effects of serpentinization on density
461 and magnetic susceptibility; a petrophysical model. *Physics of the Earth and Planetary Interiors*
462 65: 137–157, doi: 10 .1016 /0031 -9201 (90)90082 -9.

463
464 Tucholke, B. E., Lin, J., Kleinrock, M. C., 1998. Megamullions and mullion structure defining
465 oceanic metamorphic core complexes on the Mid-Atlantic. *J. Geophys. Res.* 103: 9857–9866,
466 doi: 10.1029/98JB00167.

467

468

469 **Figures captions**

470

471 **Fig. 1:** Bathymetry of the LCHF. (A) Regional, ship-based bathymetry of the Atlantis Massif, at
472 the inside corner of the intersection between the Mid-Atlantic Ridge and the Atlantis Transform
473 Fault. (B) Detailed bathymetry of Lost City and its surroundings. (C) Lost City seen from various
474 angles, respectively corresponding to the red arrows on B. The Poseidon complex and the near
475 vertical cliff marking the fault immediately east of the site are clearly apparent.

476
477 **Fig. 2:** Equivalent magnetization and magnetic anomaly of the LCHF (Same projections as in
478 Fig. 1C). (A) Equivalent magnetization resulting from the Bayesian inversion and draped on the
479 site high-resolution bathymetry. (B) RTP anomaly recomputed in the geometry of the experiment
480 using this magnetization and a vertical geomagnetic field. The Poseidon complex and the
481 northeastern fault are associated with the highest anomaly amplitude, whereas the rest of the site
482 is characterized by weak positive magnetic signature.

483
484 **Fig. 3:** Geometry of the magnetite distribution at LCHF (Same projections as in Fig. 1C). (A)
485 Contour of the plumbing system lower interface with reference to its magnetite distribution along
486 two across-site profiles (red lines), producing an anomaly with a satisfying shape. The high-
487 resolution bathymetry outline (black lines) is also added. Seawater infiltration occurs at the faults
488 intersection with the seafloor and a weakly magnetized plumbing system is sufficient to account
489 for the observed anomaly amplitude. (B) Synthetic anomaly produced in the geometry of the
490 experiment assuming a vertical geomagnetic field and a 2 A/m magnetized plumbing system.
491 This model fits with the observed RTP anomaly and reveals low magnetite concentration
492 resulting from low-temperature serpentinization reactions.

493
494 **Fig. 4:** Sections of the LCHF showing the potential propagation of hydrothermal activity. (A)
495 Proposed geometry of the plumbing system along the two across-site profiles. Seawater
496 infiltration initiates low-temperature serpentinization reaction, i.e., the production of a small
497 amount of magnetite. (B) map view of the site. The highest magnetization area encompasses the
498 Poseidon complex and the fault to the northeast, suggesting a progressive shift of hydrothermal
499 activity upslope.

500
501
502
503
504
505
506
507
508
509
510
511
512
513
514
515
516
517
518
519
520
521
522

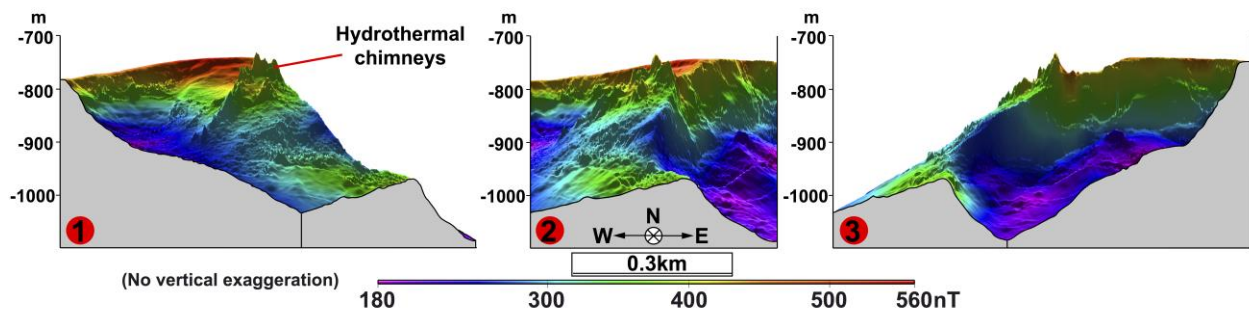
**Magnetic exploration of a low-temperature ultramafic-hosted hydrothermal
site (Lost City, 30°N, MAR)**

Florent Szitkar, Maurice A. Tivey, Deborah S. Kelley, Jeffrey A. Karson, Gretchen L. Früh-
Green, Alden R. Denny

Supplementary material

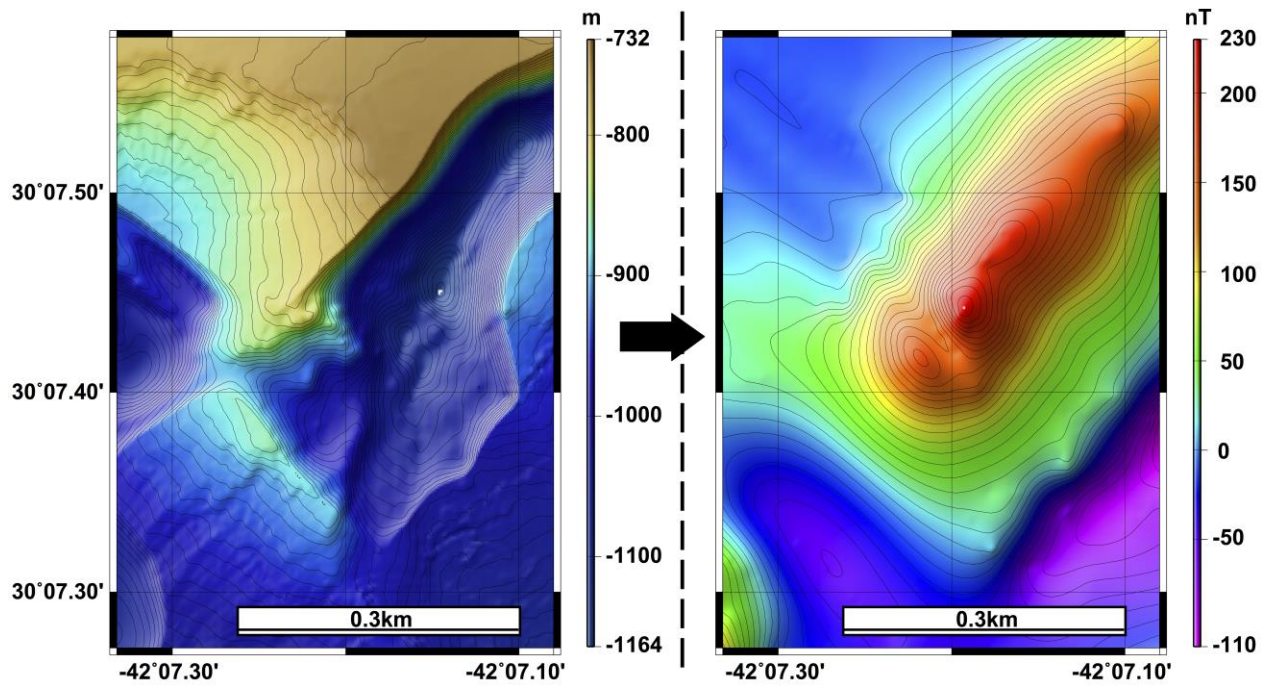
This supplementary file includes two figures, numbered S1 and S2, and the accompanying
captions.

523
524
525
526
527
528
529



530
531
532
533

Figure S1: Synthetic anomaly produced by a uniformly, 1A/m-magnetized seafloor in the geometry of the experiment. The result does not match the observed anomaly, confirming that the site is not magnetically neutral.



534
 535 **Figure S2:** Left: Lower plumbing system interface producing an anomaly with the right shape, assuming a constant
 536 seafloor magnetization. Right: Synthetic anomaly produced by a 1A/m magnetized seafloor in the geometry of the
 537 experiment, assuming the above-mentioned plumbing system. The lower interface is located at unrealistic depths, as
 538 an infinitely thick plumbing system does not generate sufficient anomaly amplitude. Magnetization variations are
 539 required.